Rotation effect on the thermodynamics of QCD matter*

Fei Sun (孙飞)[1,2,3†] Shuang Li (李双)[1,3‡] Rui Wen (温睿)[2§] Anping Huang (黄安平)[2¶] Wei Xie (谢伟)[1,3#]

[1]Department of Physics, China Three Gorges University, Yichang 443002, China
[2]School of Nuclear Science and Technology, University of Chinese Academy of Sciences, Beijing 100049, China
[3]Center for Astronomy and Space Sciences, China Three Gorges University, Yichang 443002, China

Abstract: In this study, we investigated the impact of rotation on the thermodynamic properties of QCD matter using the three-flavor NJL model. We examined the dependencies of key thermodynamic quantities, such as the trace anomaly, specific heat, speed of sound, angular momentum, and moment of inertia, on temperature, quark chemical potential, and angular velocity. Our main finding is that the speed of sound exhibits a nonmonotonic behavior as the angular velocity varies.

Keywords: QCD, rotation, thermodynamics

DOI: 10.1088/1674-1137/add25e **CSTR:** 32044.14.ChinesePhysicsC.49093105

I. INTRODUCTION

In recent years, there has been growing interest in studying matter under extreme conditions, particularly in the context of intense rotational scenarios within the field of Quantum Chromodynamics (QCD). QCD matter produced in non-central collisions exhibits a non-negligible angular momentum on the order of $10^4 \sim 10^5\hbar$, with local angular velocities in the range of 0.01~0.1 GeV [1−5]. The orbital angular momentum of the Quark-Gluon Plasma (QGP) can be transferred to the spin of its constituent particles through spin-orbit coupling, a phenomenon known as the Barnett effect [6, 7]. Consequently, quarks and anti-quarks become polarized along the direction of the reaction plane. In 2005, Liang and Wang [1] predicted that spin–orbit coupling would lead to the polarization of strange quarks produced in non-central heavy ion collisions. Subsequently, in 2008, Becattini and colleagues [3] highlighted that, within a hydrodynamic framework, local thermodynamic equilibrium implies a relationship between spin polarization and the structure of rotational flow. Significant progress has also been made in theoretical investigations of QCD matter under rotation, which has attracted considerable attention in recent years. Previous studies have also explored various phenomena such as pion superfluidity [8−10], ρ meson superconductivity [11, 12], and chiral and deconfinement transitions [13−24].

Experimentally, in 2017, the STAR Collaboration published the first observation of global polarization resulting from non-central heavy-ion collisions [25]; in 2020, the ALICE Collaboration reported spin alignment of vector mesons ϕ and K^{*0} [26]; and in 2023, the STAR Collaboration also measured the spin alignment of ϕ and K^{*0} [27]. Additionally, there have been advancements in lattice simulations of rotating systems [28−32]. These advances have led to the exploration of numerous spin-related quantum phenomena and remarkably strong fluid vorticity structures. For example, hydrodynamic simulations have been widely used to investigate vorticity and spin polarization in heavy-ion collisions. Hydrodynamic [33−47] and transport [48−56] models have made significant progress in the study of vorticity and polarization observables.

QCD thermodynamic quantities reflect the physical characteristics of the QCD phase transition. Knowledge of these quantities at finite temperature, chemical potential, and angular velocity is essential for studying non-central collisions. Some thermodynamic quantities, such as the trace anomaly and speed of sound, are sensitive to

Received 20 December 2024; Accepted 30 April 2025; Published online 1 May 2025

* Supported by the National Natural Science Foundation of China (NSFC) (12375137, 12205309), the Yichang Natural Science Foundation (A25-3-002), the start-up funding from University of Chinese Academy of Sciences (UCAS), and the Fundamental Research Funds for the Central Universities

† E-mail: sunfei@ctgu.edu.cn
‡ E-mail: lish@ctgu.edu.cn
§ E-mail: rwen@ucas.ac.cn
¶ E-mail: huanganping@ucas.ac.cn
# E-mail: xiewei@ctgu.edu.cn

the phase transition and serve as potential signals for experimentally studying the transition and identifying the critical endpoint. Experimental determination of the speed of sound in QGP was proposed in [57−61]. Besides, QCD thermodynamic quantities, such as pressure and speed of sound, are crucial inputs for hydrodynamic simulations and transport models [62−65]. Therefore, it is important to investigate the rotation effect on the thermodynamics of strong interaction matter.

According to lattice simulations [66, 67] and functional renormalization group theory [68−71], at low momentum or renormalization group scale, the gluons are decoupled from the system owing to the finite mass gap. The QCD system, which includes degrees of freedom of quarks and gluons, is transformed into a system composed by quarks and hadrons, which can be described by low energy effective field models. These models, such as the Nambu–Jona-Lasinio (NJL) model [14, 72−76] and quark meson model [77−79], offer alternative approaches to exploring strongly interacting matter, capturing essential features of QCD and providing insights into the QCD phase structure at finite temperature, density, and angular velocity.

In this study, we employed the three-flavor NJL model to analyze the thermodynamic properties of strongly interacting matter under rotation, including the speed of sound, angular momentum, and moment of inertia. This paper is organized as follows. In Sec. II, we introduce the formalism of the three-flavor NJL model and derive detailed expressions for thermodynamics in the presence of rotation. In Sec. III, we present numerical results and discussions on thermodynamic quantities. Finally, in Sec. IV, we summarize our findings and conclude the paper.

II. FORMALISM

First, we provide a brief overview of the foundation for studying rotating matter within an effective model. The general approach is to conduct the study in a reference frame that rotates with the system [14, 23, 80, 81]. In this frame of reference, rotation can be described in terms of an external gravitational field. The structure of space-time in a rotating frame is represented by the metric tensor, which reads

$$g_{\mu\nu}=\begin{pmatrix} 1-\vec{v}^2 & -v_1 & -v_2 & -v_3 \\ -v_1 & -1 & 0 & 0 \\ -v_2 & 0 & -1 & 0 \\ -v_3 & 0 & 0 & -1 \end{pmatrix}, \tag{1}$$

where v_i is the velocity. Our starting point is the partition function

$$\mathcal{Z}=\int D[\bar{\psi}]D[\psi]\mathrm{e}^{-\mathrm{i}S}, \tag{2}$$

where S denotes the quark action, which is the integration of the Lagrangian density $\mathcal{L}$. When extending to the case of rotating fermions [14, 80, 82] with non-zero chemical potential, the Lagrangian in the three-flavor NJL model is given by

$$\begin{aligned}\mathcal{L}=&\bar{\psi}\left(\mathrm{i}\bar{\gamma}^{\mu}(\partial_{\mu}+\Gamma_{\mu})-m+\gamma^0\mu\right)\psi\\&+G\sum_{a=0}^{8}\left(\bar{\psi}\lambda^a\psi\right)^2\\&-K\{\det[\bar{\psi}(1+\gamma^5)\psi]+\det[\bar{\psi}(1-\gamma^5)\psi]\},\end{aligned} \tag{3}$$

where ψ is the quark field; $\bar{\gamma}^{\mu}=e_a^{\ \mu}\gamma^a$ with $e_a^{\ \mu}$ denoting the tetrads for spinors and γ^a denoting the gamma matrix; Γ_{μ} is defined as $\Gamma_{\mu}=\frac{1}{4}\times\frac{1}{2}[\gamma^a,\gamma^b]\,\Gamma_{ab\mu}$, which is the spinor connection, where $\Gamma_{ab\mu}=\eta_{ac}(e^c_{\ \sigma}G^{\sigma}_{\ \mu\nu}e_b^{\ \nu}-e_b^{\ \nu}\partial_{\mu}e^c_{\ \nu})$; $G^{\sigma}_{\ \mu\nu}$ is the affine connection determined by $g^{\mu\nu}$; m is the bare quark mass matrix; μ denotes the chemical potential; G represents the coupling constant of the four-point interaction term; and $\lambda^a(a=1,...8)$ are the Gell-Mann matrices in the flavor space. The last term corresponds to the 't Hooft interaction with coupling strength K, which is a determinant in the flavor space. Considering a system with an angular velocity along the fixed z-axis, then $\vec{v}=\vec{\omega}\times\vec{x}$. By choosing $e^a_{\ \mu}=\delta^a_{\ \mu}+\delta^a_{\ i}\delta^0_{\ \mu}v_i$ and $e_a^{\ \mu}=\delta_a^{\ \mu}-\delta_a^{\ 0}\delta_i^{\ \mu}v_i$, and expanding the Lagrangian to first-order in angular velocity, we obtain the following expression:

$$\begin{aligned}\mathcal{L}=&\bar{\psi}\left[\mathrm{i}\gamma^{\mu}\partial_{\mu}-m+\gamma^0\mu\right]\psi\\&+\bar{\psi}\left[(\gamma^0)^{-1}\left((\vec{\omega}\times\vec{x})\cdot\left(-\mathrm{i}\vec{\partial}\right)+\vec{\omega}\cdot\vec{S}_{4\times4}\right)\right]\psi\\&+G\sum_{a=0}^{8}\left(\bar{\psi}\lambda^a\psi\right)^2\\&-K\{\det[\bar{\psi}(1+\gamma^5)\psi]+\det[\bar{\psi}(1-\gamma^5)\psi],\end{aligned} \tag{4}$$

where $\vec{S}_{4\times4}=\frac{1}{2}\begin{pmatrix}\vec{\sigma} & 0\\ 0 & \vec{\sigma}\end{pmatrix}$ is the spin operator. Applying the technique of the path integral formulation for the theory of Grassmann variables and the mean field approximation, linearization of 4-quark and 6-quark interactions is achieved, yielding the following expression for $\log\mathcal{Z}$:

$$\log\mathcal{Z}=\frac{1}{T}\int \mathrm{d}^3x\left(2G\sum_f\langle\bar{\psi}_f\psi_f\rangle^2-4K\prod_f\langle\bar{\psi}_f\psi_f\rangle\right)+\sum_f\log\det\frac{D_f^{-1}}{T}. \tag{5}$$

The inverse fermion propagator D^{-1} in Eq. (5) can be derived as follows:

$$D^{-1}=\gamma^0\left(-\mathrm{i}\omega_l+\left(n+\frac{1}{2}\right)\omega+\mu\right)-M-\vec{\gamma}.\vec{p}, \tag{6}$$

where we have introduced the Matsubara frequency, $\omega_l=-\mathrm{i}\,p_0=(2l+1)\pi T$, at temperature T, and M denotes the dynamical mass of the quark,

$$M_q=m_q+(2K\langle\bar{s}s\rangle-4G)\langle\bar{q}q\rangle, \tag{7}$$

$$M_s=m_s-4G\langle\bar{s}s\rangle+2K\langle\bar{q}q\rangle^2\,. \tag{8}$$

To find solutions of the Dirac equation, we start by choosing a complete set of commutating operators consisting of $\hat{H}$, which can be obtained from Eq. (4) by using the relation $\mathcal{H}=\bar{\psi}\left(\mathrm{i}\gamma^0\partial_0\right)\psi-\mathcal{L}$, momentum in the z-direction $\hat{p}_z$, square of transverse momentum $\hat{p}_t^2$, z-component of the total angular momentum $\hat{J}_z$, and transverse helicity $\hat{h}_t$, where $\hat{h}_t=\gamma^5\gamma^3\vec{p}_t\cdot\vec{S}$, and $\gamma^5=\mathrm{i}\gamma^0\gamma^1\gamma^2\gamma^3$. By solving the eigenvalue equations of the complete set of commuting operators $\{\hat{H},\ \hat{p}_z,\ \hat{p}_t^2,\hat{J}_z,\ \hat{h}_t\}$, we obtain the positive and negative energy solutions of the Dirac field as follows. In cylindrical coordinates, the general spinor eigenstates can be expressed as

$$u=\sqrt{\frac{E+m}{4E}}\begin{pmatrix}\mathrm{e}^{\mathrm{i}p_zz}\mathrm{e}^{\mathrm{i}n\theta}J_n(p_tr)\\ s\mathrm{e}^{\mathrm{i}p_zz}\mathrm{e}^{\mathrm{i}(n+1)\theta}J_{n+1}(p_tr)\\ \frac{p_z-\mathrm{i}sp_t}{E+m}\mathrm{e}^{\mathrm{i}p_zz}\mathrm{e}^{\mathrm{i}n\theta}J_n(p_tr)\\ \frac{-sp_z+\mathrm{i}p_t}{E+m}\mathrm{e}^{\mathrm{i}p_zz}\mathrm{e}^{\mathrm{i}(n+1)\theta}J_{n+1}(p_tr)\end{pmatrix}, \tag{9}$$

$$v=\sqrt{\frac{E+m}{4E}}\begin{pmatrix}\frac{p_z-\mathrm{i}sp_t}{E+m}\mathrm{e}^{-\mathrm{i}p_zz}\mathrm{e}^{\mathrm{i}n\theta}J_n(p_tr)\\ \frac{-sp_z+\mathrm{i}p_t}{E+m}\mathrm{e}^{-\mathrm{i}p_zz}\mathrm{e}^{\mathrm{i}(n+1)\theta}J_{n+1}(p_tr)\\ \mathrm{e}^{-\mathrm{i}p_zz}e^{\mathrm{i}n\theta}J_n(p_tr)\\ -s\mathrm{e}^{-\mathrm{i}p_zz}\mathrm{e}^{\mathrm{i}(n+1)\theta}J_{n+1}(p_tr)\end{pmatrix}. \tag{10}$$

Here, $s=\pm1$ represent the transverse helicity values and n denotes the z-direction angular momentum quantum number. After the summation of all the Matsubara frequencies and following the general approach of finite temperature fields [83], it can be shown that the grand thermodynamic potential ($\Omega=-\frac{T}{V}\log\mathcal{Z}$) takes the following form:

$$\begin{aligned}\Omega=&\,2G\left(2\langle\bar{q}q\rangle^2+\langle\bar{s}s\rangle^2\right)-4K\langle\bar{q}q\rangle^2\langle\bar{s}s\rangle-\frac{3}{2\pi^2}\sum_{n=-\infty}^{\infty}\int_0^{\Lambda}p_t\mathrm{d}p_t\int_{-\sqrt{\Lambda^2-p_t^2}}^{\sqrt{\Lambda^2-p_t^2}}\mathrm{d}p_z\left(\left(J_{n+1}(p_tr)^2+J_n(p_tr)^2\right)\left(E_q-\left(\frac{1}{2}+n\right)\omega\right)\right)\\
&-\frac{3}{2\pi^2}\sum_{n=-\infty}^{\infty}\int_0^{\infty}p_t\mathrm{d}p_t\int_{-\infty}^{\infty}\mathrm{d}p_z\left(\left(J_{n+1}(p_tr)^2+J_n(p_tr)^2\right)T\left\{\log\left(\mathrm{e}^{-\frac{-\mu_q+E_q-\left(\frac{1}{2}+n\right)\omega}{T}}+1\right)+\log\left(\mathrm{e}^{-\frac{\mu_q+E_q-\left(\frac{1}{2}+n\right)\omega}{T}}+1\right)\right\}\right)\\
&-\frac{3}{4\pi^2}\sum_{n=-\infty}^{\infty}\int_0^{\Lambda}p_t\mathrm{d}p_t\int_{-\sqrt{\Lambda^2-p_t^2}}^{\sqrt{\Lambda^2-p_t^2}}\mathrm{d}p_z\left(\left(J_{n+1}(p_tr)^2+J_n(p_tr)^2\right)\left(E_s-\left(\frac{1}{2}+n\right)\omega\right)\right)\\
&-\frac{3}{4\pi^2}\sum_{n=-\infty}^{\infty}\int_0^{\infty}p_t\mathrm{d}p_t\int_{-\infty}^{\infty}\mathrm{d}p_z\left(\left(J_{n+1}(p_tr)^2+J_n(p_tr)^2\right)T\left\{\log\left(\mathrm{e}^{-\frac{-\mu_s+E_s-\left(\frac{1}{2}+n\right)\omega}{T}}+1\right)+\log\left(\mathrm{e}^{-\frac{\mu_s+E_s-\left(\frac{1}{2}+n\right)\omega}{T}}+1\right)\right\}\right).\end{aligned} \tag{11}$$

Here, the quark quasiparticle energy is $E_f=\sqrt{M_f^2+p_t^2+p_z^2}$. For simplicity, we also introduce the quark quasiparticle energy under rotation:

$$E_{f,n}=E_f-\left(\frac{1}{2}+n\right)\omega. \tag{12}$$

Note that the expression for the grand thermodynamic potential above contains an explicit cutoff dependence due to the nonrenormalizability of the NJL model. Here, the thermodynamic potential naturally separates into a vacuum contribution and a temperature-dependent matter part, which is helpful for calculating thermodynamic quantities. The three-momentum cutoff in the vacuum part should be chosen to reproduce observables, such as the pion mass and pion decay constant. In principle, the cutoff in the matter part should be infinity. Here, Λ is the

three-momentum cutoff of the vacuum part in the potential.

Then, we consider the gap equations to minimize the grand potential. The dynamical quark mass M_f can be determined by solving the stationary condition. We also require the solutions to satisfy the condition of the minimum of the potential:

$$\frac{\partial\Omega}{\partial\langle\bar{q}q\rangle}=\frac{\partial\Omega}{\partial\langle\bar{s}s\rangle}=0, \tag{13}$$

$$\frac{\partial^2\Omega}{\partial\langle\bar{q}q\rangle^2}>0,\ \ \frac{\partial^2\Omega}{\partial\langle\bar{s}s\rangle^2}>0, \tag{14}$$

which leads to the following coupled gap equations:

$$\begin{aligned}0=&\left(8G\langle\bar{q}q\rangle-8K\langle\bar{s}s\rangle\langle\bar{q}q\rangle\right)-\frac{3}{\pi^2}\sum_{n=-\infty}^{\infty}\int_0^{\Lambda}p_t\mathrm{d}p_t\int_{-\sqrt{\Lambda^2-p_t^2}}^{\sqrt{\Lambda^2-p_t^2}}\mathrm{d}p_z\left(\left(J_{n+1}(p_tr)^2+J_n(p_tr)^2\right)\right.\\&\times\left(\frac{(-2G+K\langle\bar{s}s\rangle)M_q}{E_q}+\frac{K\langle\bar{q}q\rangle M_s}{E_s}\right)+\frac{3}{\pi^2}\sum_{n=-\infty}^{\infty}\int_0^{\infty}p_t\mathrm{d}p_t\int_{-\infty}^{\infty}\mathrm{d}p_z\left(\left(J_{n+1}(p_tr)^2+J_n(p_tr)^2\right)\right.\\&\times\left\{\frac{(-2G+K\langle\bar{s}s\rangle)M_q}{E_q}\left[n_f(E_{q,n},T,\mu)+\bar{n}_f(E_{q,n},T,\mu)\right]+\frac{K\langle\bar{q}q\rangle M_s}{E_s}\left[n_f(E_{s,n},T,\mu)+\bar{n}_f(E_{s,n},T,\mu)\right]\right\},\end{aligned} \tag{15}$$

$$\begin{aligned}0=&\left(4G\langle\bar{s}s\rangle-4K\left(\langle\bar{q}q\rangle\right)^2\right)-\frac{3}{\pi^2}\sum_{n=-\infty}^{\infty}\int_0^{\Lambda}p_t\mathrm{d}p_t\int_{-\sqrt{\Lambda^2-p_t^2}}^{\sqrt{\Lambda^2-p_t^2}}\mathrm{d}p_z\left(J_{n+1}(p_tr)^2+J_n(p_tr)^2\right)\\&\times\left(\frac{K\langle\bar{q}q\rangle M_q}{E_q}-\frac{GM_s}{E_s}\right)+\frac{3}{\pi^2}\sum_{n=-\infty}^{\infty}\int_0^{\infty}p_t\mathrm{d}p_t\int_{-\infty}^{\infty}\mathrm{d}p_z\left(J_{n+1}(p_tr)^2+J_n(p_tr)^2\right)\\&\times\left\{\frac{K\langle\bar{q}q\rangle M_q}{E_q}\left[n_f(E_{q,n},T,\mu)+\bar{n}_f(E_{q,n},T,\mu)\right]-\frac{GM_s}{E_s}\left[n_f(E_{s,n},T,\mu)+\bar{n}_f(E_{s,n},T,\mu)\right]\right\},\end{aligned} \tag{16}$$

where n_f and $\bar{n}_f$ denote the quark and anti-quark distribution functions:

$$n_f(E_{f,n},T,\mu)=\frac{1}{\mathrm{e}^{\frac{E_{f,n}-\mu}{T}}+1}, \tag{17}$$

$$\bar{n}_f(E_{f,n},T,\mu)=\frac{1}{\mathrm{e}^{\frac{E_{f,n}+\mu}{T}}+1}. \tag{18}$$

This set of coupled equations is then solved for the fields as functions of temperature T, quark chemical potential μ, and angular velocity ω. We now turn to the thermodynamics of the rotating system. When extending to a rotating system, vorticity should be considered an additional intensive thermodynamic quantity necessary for describing the local fluid. As a result, some corrections may need to be applied to the energy density [16, 84, 85]:

$$\varepsilon=-p+Ts+\mu n+\omega J. \tag{19}$$

Here, n denotes the quark number density, and J presents the (polarization) angular momentum density.

From standard thermodynamic relations, the pressure, angular momentum density (related to polarization), and quark number density are given as follows (the angular velocity can be regarded as an "effective chemical potential," allowing the angular momentum to be defined as the derivative of the grand canonical potential with respect to the angular velocity):

$$p=\Omega(T=0,\mu=0,\omega=0)-\Omega(T,\mu,\omega), \tag{20}$$

$$s=-\left(\frac{\partial\Omega}{\partial T}\right)_{\mu,\omega}, \tag{21}$$

$$n=-\left(\frac{\partial\Omega}{\partial\mu}\right)_{T,\omega}, \tag{22}$$

$$J=-\left(\frac{\partial\Omega}{\partial\omega}\right)_{T,\mu}, \tag{23}$$

where, to obtain a physical pressure, we have renormalized the thermodynamic potential. The subscript indicates that the chemical potential and angular velocity are held fixed during the partial differentiation. The trace an-

omaly is defined as

$$\Theta = \varepsilon - 3p. \tag{24}$$

For each flavor, the explicit formulae of entropy and quark number densities, as well as the angular momentum along the z-axis, are listed in A.

After obtaining the expression of the angular momentum, we can directly obtain the moment of inertia of the rotating system as

$$I = \frac{1}{\omega}\left(-\frac{\mathrm{d}\Omega}{\mathrm{d}\omega}\right) = \frac{J}{\omega}. \tag{25}$$

For the description of the expansion of dense matter created in heavy ion collisions, a fundamental quantity that determines the expansion of hot dense matter is the speed of sound,

$$c_s^2 = \frac{\mathrm{d}p}{\mathrm{d}\epsilon}, \tag{26}$$

and another quantity of interest is the specific heat,

$$C_V = \frac{\mathrm{d}\epsilon}{\mathrm{d}T}. \tag{27}$$

Here, we have not listed their detailed expressions, as they can be readily obtained from the formulas above.

III. NUMERICAL RESULTS AND DISCUSSIONS

A. Dynamical quark mass and chiral transition

In this section, we present our numerical results for the dynamical quark mass and chiral transition in the three-flavor NJL model under rotation. In our calculations, the input parameters in the NJL model are the coupling constants G, light quark mass m_q (we ignore isospin breaking effects and work with $m_u = m_d = m_q$), strange quark mass m_s, three-momentum cutoff Λ, and 't Hooft term coupling constant. We used the model parameters reported in Ref. [86], which were estimated by fitting according to the following observations: $m_\pi = 138$ MeV, $f_\pi = 92$ MeV, $m_K = 495$ MeV and $m_{\eta'} = 958$ MeV. The input parameters were set as follows: $m_q = 0.005$ GeV, $m_s = 0.1283$ GeV, $G = 3.672$ GeV^{-2}, $K = 59.628$ GeV^{-5}, $\Lambda = 0.6816$ GeV. Throughout this paper, unless otherwise specified, the radius r is assumed to be 0.1 GeV^{-1}.

We present the evolution of the light quark mass with respect to T and ω in Fig. 1(a) and the strange quark mass in Fig. 1(b). Note that there is a decrease in mass as the temperature or angular velocity increases, indicating the restoration of chiral symmetry at high temperatures or

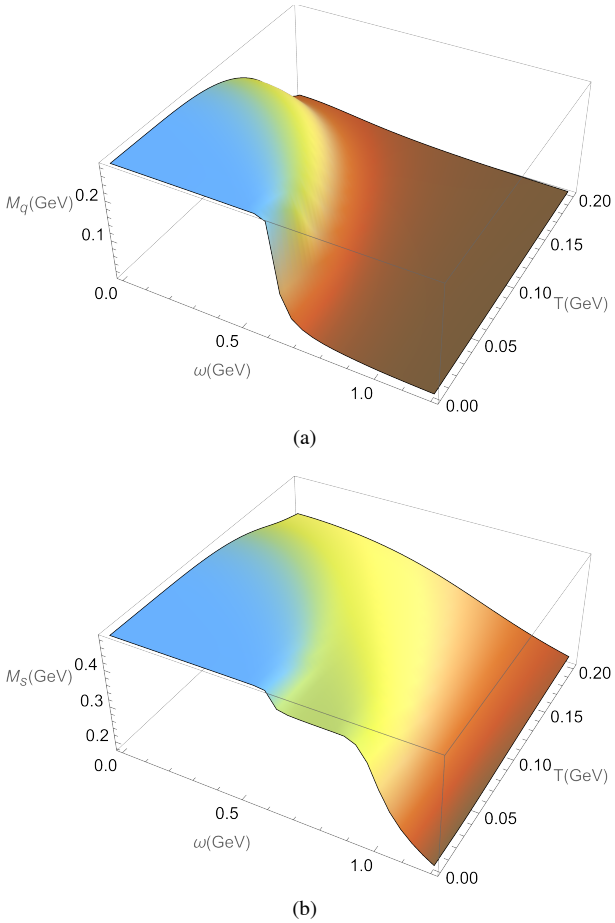

Fig. 1. (color online) Effective masses of light and strange quarks as functions of temperature T and angular velocity ω for$\mu = 0.01$ GeV.

large angular velocities. Notably, rapid transitions occur in the low temperature, high angular velocity region, while only very gradual changes are observed in the high temperature, low angular velocity region. It is evident that, at very low fixed temperatures, chiral symmetry restoration undergoes a rapid transition with increasing rotation. This behavior can be interpreted as a continuous crossover becoming steeper with rising angular velocity, eventually evolving into a sharp transition at high angular velocities. By comparing the critical angular velocities ω_c for the light and strange quarks, it can be concluded that the decrease is faster for the light quark, which suggests that the chiral symmetry restoration is more efficient for the light quark than for the strange quark.

Then, we extended the investigation on the effective quark mass to the $\omega - \mu$ plane. In Fig. 2, we show the evolution of the effective masses for the light and strange quarks as functions of the angular velocity and quark chemical potential. Clearly, at sufficiently large angular velocity or (and) sufficiently large quark chemical potential, the quark effective mass is very small. When the an-

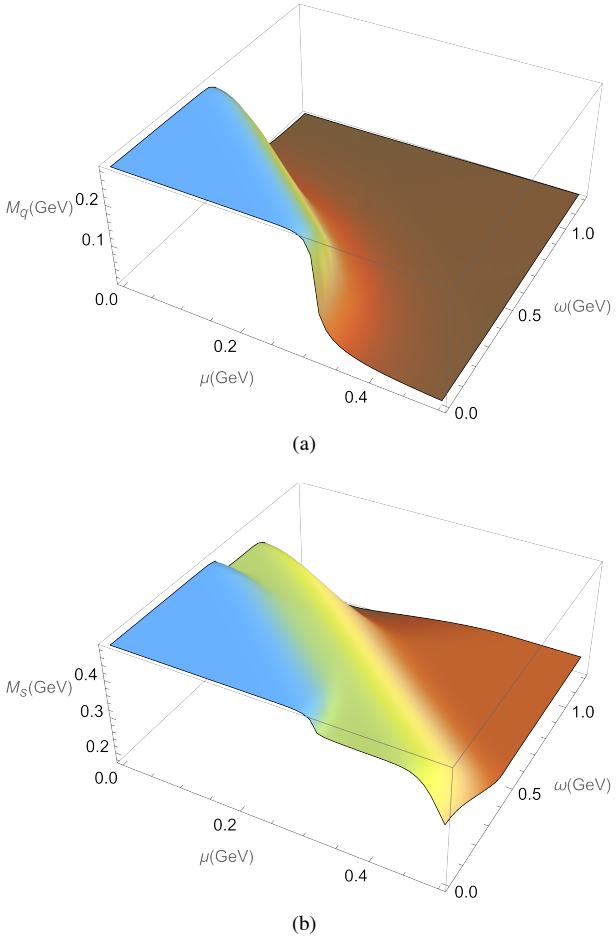

Fig. 2. (color online) Effective masses of light and strange quarks as functions of angular velocity ω and quark chemical potential μ for T=0.01 GeV.

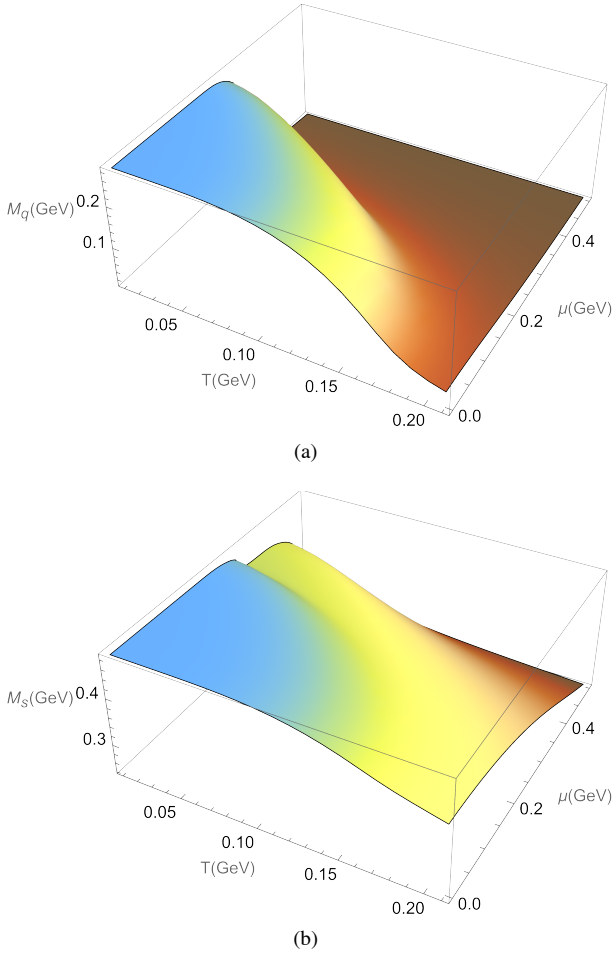

Fig. 3. (color online) Effective masses of light and strange quarks as functions of temperature T and quark chemical potential μ for $\omega = 0.1$ GeV.

gular velocity is small, there is an abrupt change for the light quark around $\mu = 0.3$ GeV, whereas for the strange effective quark, there are two regions that quickly change. Note also that there are similar transition regions of the small quark chemical potential and large angular velocity in the left rear side of the figure.

The temperature and chemical potential dependence of the light and strange quark effective masses at $\omega = 0.1$ GeV is depicted in Fig. 3. Note that, at low temperature and small quark chemical potential, chiral symmetry is spontaneously broken. As the temperature or quark chemical potential increases, the effective mass of the strange quark shows only mild dependence on these variables, while the light quark mass is more sensitive in comparison. In the low temperature region, the effective mass of the light quark exhibits a sharp drop at certain values of μ with increasing μ. Note also that at high temperature or large quark chemical potential, the effective masses of these quarks become small. At sufficiently high temperature or large chemical potential, the effective mass of the light quark approaches its current mass, while the strange quark retains a relatively large effective mass. This indicates that the current quark mass plays an important role in the chiral transition.

The quark condensate $\langle\bar{q}q\rangle$ or $\langle\bar{s}s\rangle$ is often treated as an order parameter for spontaneous chiral symmetry breaking. The temperature-dependence of the order parameters for different values of the rotational speed are shown in Fig. 4. Note that there is a rapid cross-over with a critical angular velocity at approximately 0.6 GeV and 1.0 GeV for the light and strange quark condensates, respectively. At low temperatures and small angular velocities, the chiral symmetry is spontaneously broken. At high temperatures or (and) large angular velocities, chiral symmetry may gradually be restored.

The chiral phase transition temperature in the presence of angular velocity is shown in Fig. 5. The definition of T_{pc} in this context is determined by the maximum of $\left|\frac{\mathrm{d}\phi_f}{\mathrm{d}T}\right|$, where $f = u, d, s$ and $\phi_u = \phi_d = \langle\bar{q}q\rangle, \phi_s = \langle\bar{s}s\rangle$. Fig. 5 shows that the pseudocritical temperature decreases as the angular velocity becomes larger. At small angular velocity, the pseudocritical temperature of the strange quark is approximately 0.1 GeV larger than that

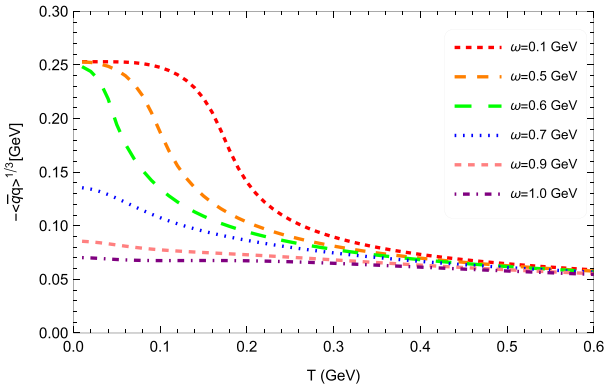

(a)

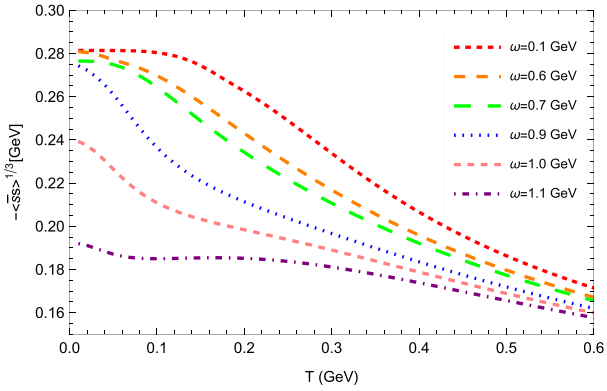

(b)

Fig. 4. (Color online) Condensates of light and strange quarks as functions of temperature for different values of the rotational speed.

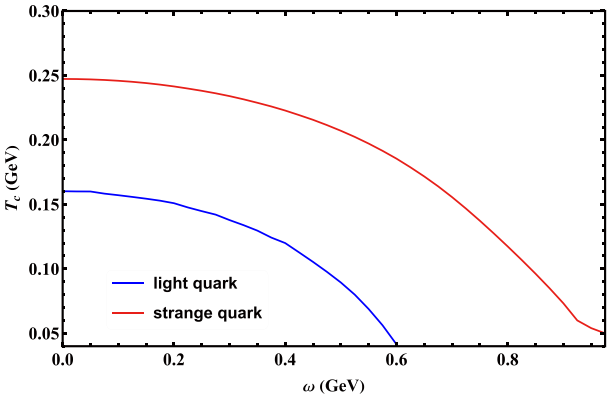

Fig. 5. (color online) Pseudocritical temperatures for chiral transition of rotating quark matter as functions of the angular velocity.

of the light quark, even at a large angular velocity around 0.6 GeV, where the pseudocritical temperature of the light quark is significantly small and, by contrast, the pseudocritical temperature of strange is still notably large. Thus, the conclusion appears to be that rotation can cause a significant change in the chiral transition of light quarks compared to that of the strange quark, due to the

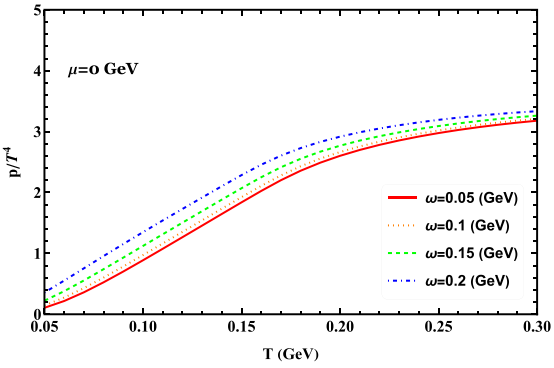

(a)

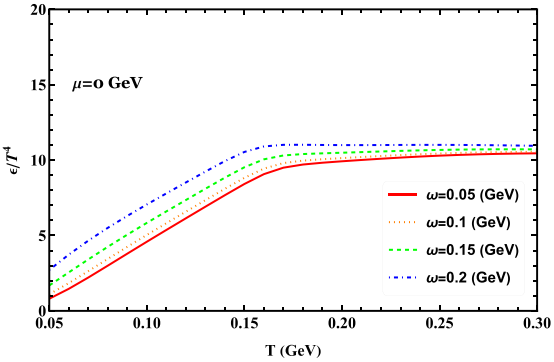

(b)

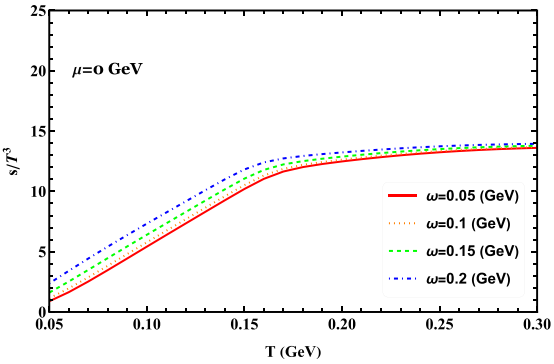

(c)

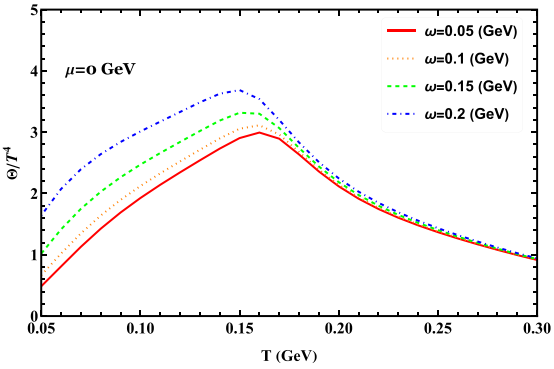

(d)

Fig. 6. (color online) Scaled pressure, energy density, entropy density, and trace anomaly as functions of temperature at zero chemical potential for different angular velocities.

heavier mass of the latter.

B. Thermodynamics results for different angular velocities at vanishing quark chemical potential

Figure 6 shows that the scaled pressure, energy, and entropy densities increase with temperature. These quantities increase rapidly with temperature and then continue to grow more gradually after passing through the transition region. The presence of rotation enhances these scaled quantities significantly at low temperatures but less noticeably at high temperatures. The scaled trace anomaly exhibits a peak in the transition region and decreases as temperature continues to rise across all angular velocities. It is clear that, at low temperatures, variations in angular velocity cause significant deviations in the scaled trace anomaly, but this effect diminishes as the temperature increases.

The specific heat is an important quantity in thermodynamics. It can be considered a response function of the phase transition. Its variation with temperature is presented in Fig. 7(a). As the angular velocity increases, the peak of the specific heat, which occurs at the transition temperature, shifts toward lower temperatures. This indicates that the transition temperature decreases with increasing angular velocity. In Fig. 7(b), the speed of sound squared increases with temperature and shows little sensitivity to the angular velocity values considered. However, this may be due to the fact that only small angular velocities were examined. It is evident that, at high temperatures, the speed of sound squared approaches the conformal limit of 1/3 across different angular velocities.

An intriguing quantity in the rotating system is the angular momentum. Fig. 8(a) displays the results of the scaled angular momentum as a function of temperature at zero chemical potential for various angular velocities. The scaled angular momentum initially increases with temperature and reaches its peak across the chiral transition region ($T \sim 150$ MeV) for all angular velocities. Beyond this temperature, it decreases with further temperature increment. The moment of inertia is also of interest in our calculations because it represents the linear response of the angular momentum of the system J to the angular velocity ω. Fig. 8(b) displays the results of the moment of inertia as a function of temperature at zero chemical potential for various angular velocities. It is evident that the scaled moment of inertia always increases with temperature for different angular velocities. Moreover, for a fixed temperature, the scaled moment of inertia becomes larger with increasing angular velocity.

C. Influence of the radius on the thermodynamics in the rotating system

In the transverse directions to the axis of rotation, the radius of rotation must be constrained by the causal condition $\omega r < 1$, resulting in a finite value. Consequently, a system of QCD matter undergoing rotation must always have a finite volume. To better understand the characteristics of QCD matter produced in non-central heavy-ion collisions, it is essential to investigate the impact of finite volume effects on thermodynamic properties. Several studies have extensively examined how system size influences thermodynamic behavior and other physical quantities [87−89].

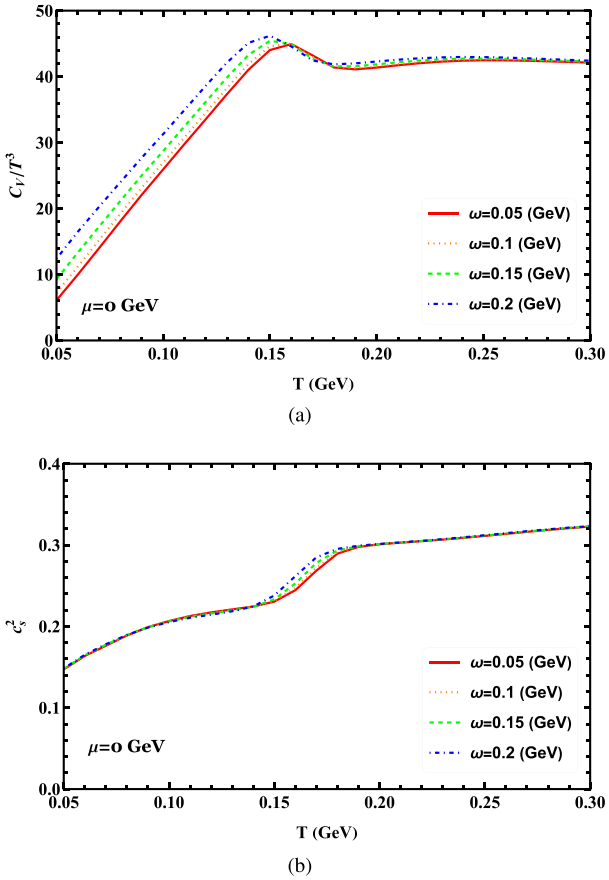

Fig. 7. (color online) Scaled specific heat and speed of sound squared as functions of temperature at zero chemical potential for different angular velocities.

In the standard NJL model, these thermodynamic quantities depend on temperature and quark chemical potential. However, in a rotating system, they should also depend on the finite size of the system. Owing to cylindrical symmetry, these quantities vary with the transverse radius r. Therefore, it is interesting to investigate how various thermodynamic quantities in strongly interacting rotating matter depend on the radius of the system. Understanding these properties as a function of the rotation radius may be relevant for future experimental observations. Additionally, the radius significantly affects angular momentum and moment of inertia. Thus, it is important to study how thermodynamic quantities in rotating QCD matter depend on the rotation radius of the sys-

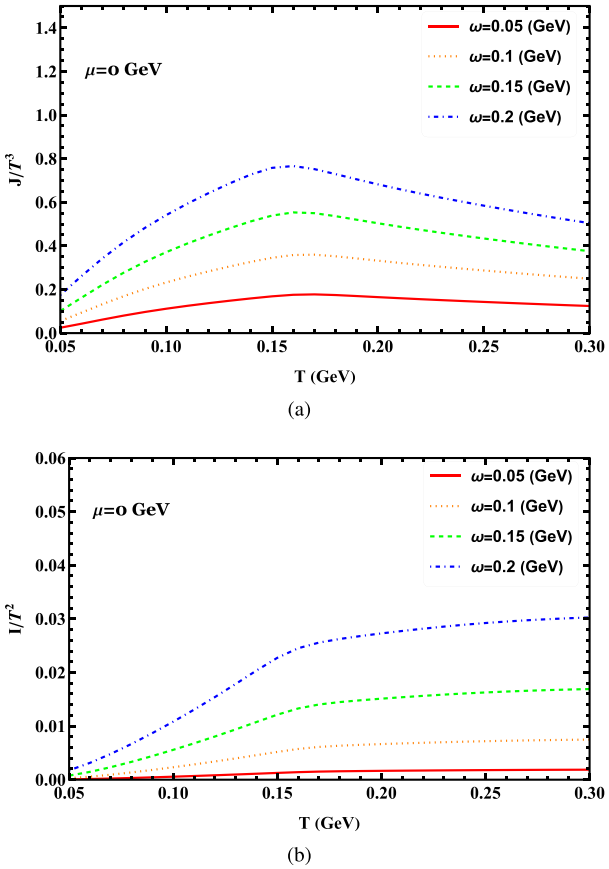

Fig. 8. (color online) Scaled angular momentum and moment of inertia as functions of temperature at zero chemical potential for different angular velocities.

tem.

We show the densities of the scaled pressure, energy, entropy, and trace anomaly as functions of temperature at zero chemical potential for different radii in Fig. 9. Note that the radius effect is noticeable and enhances these thermodynamic quantities. Although the radius effect does not qualitatively change the behavior of these quantities, even in the high-temperature region, it causes a shift in their values at a given temperature. Note also that the differences between thermodynamic quantities at different radii remain consistent, even at high temperatures.

The scaled angular momentum and moment of inertia, which are functions of temperature at zero chemical potential for different radii, are shown in Fig. 10. Fig. 10(a) shows a rapid change near the chiral transition region (around 150 MeV) for the scaled specific heat. It can be seen that the location of the peaks remains almost unchanged as the radius increases. In Fig. 10(b), it is remarkable that the speed of sound squared curves appear nearly identical around the chiral transition region. It is also observed that, at extremely high temperatures, the speed of sound squared approaches the Stefan-Boltzmann limit of 1/3 for various angular velocities. This indicates that, at high temperatures, the speed of sound squared in

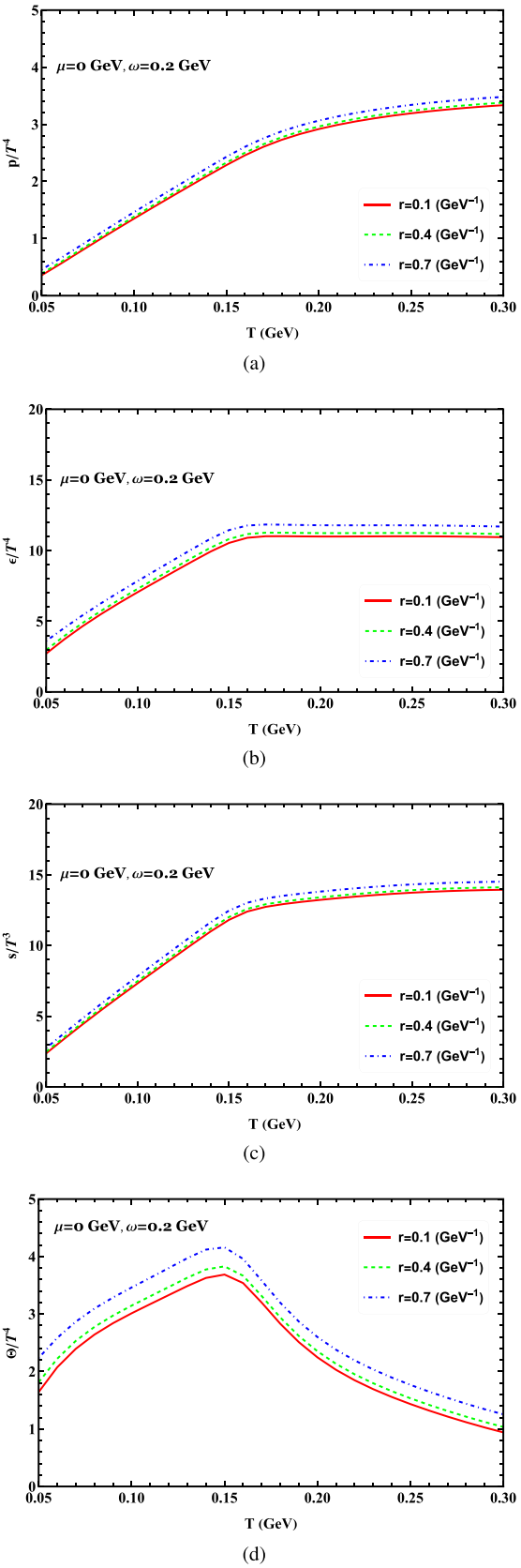

Fig. 9. (color online) Scaled pressure, energy density, entropy density, and trace anomaly as functions of temperature at zero chemical potential for different radii.

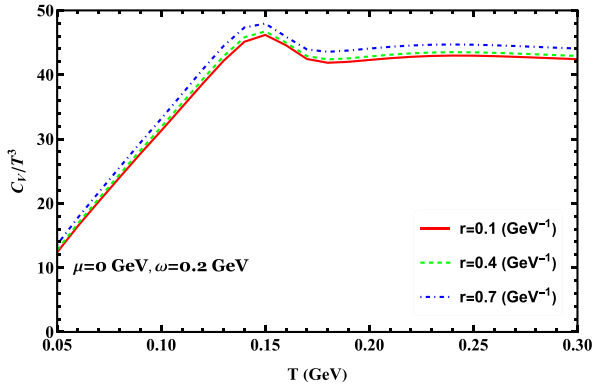

(a)

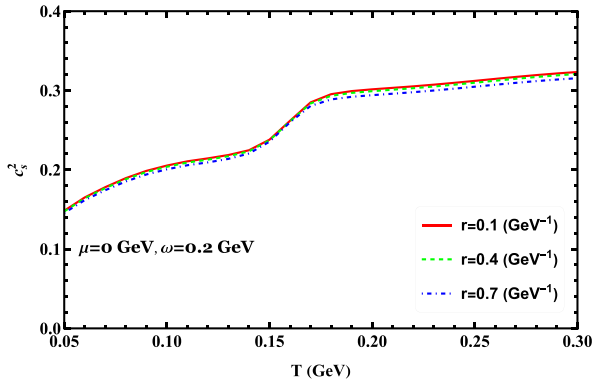

(b)

Fig. 10. (color online) Scaled specific heat and speed of sound squared as functions of temperature at zero chemical potential for different radii.

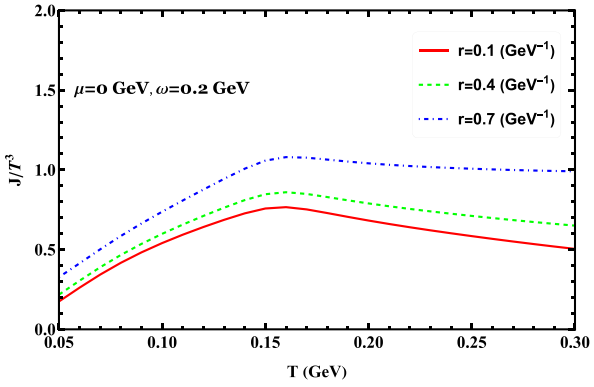

(a)

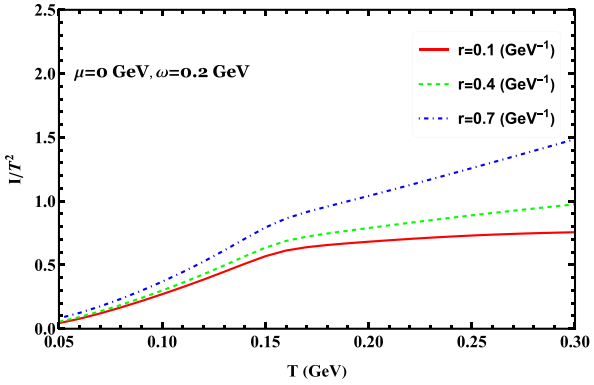

(b)

Fig. 11. (color online) Scaled angular momentum and moment of inertia as functions of temperature at zero chemical potential for different radii.

quark matter is not sensitive to the transverse radius.

It can be concluded from Fig. 11(a) that the scaled angular momentum depends on the radius. Unlike other thermodynamic quantities, angular momentum has a strong dependence on the system radius. At low temperatures, it increases smoothly with increasing radius. At high temperatures, the angular momentum becomes more pronounced. It is also evident from Fig. 11(b) that the scaled moment of inertia always increases with temperature for different radii. In the high-temperature region, the scaled moment of inertia exhibits a strong dependence on the system radius. As the temperature increases, the differences between any two curves in the figure become more pronounced for both the scaled angular momentum and scaled moment of inertia.

D. Thermodynamics in rotating system at finite chemical potential

Studying thermodynamics at finite chemical potential in a rotating system is important for understanding the QCD phase structure, modeling compact stars, and interpreting heavy ion collision experiments. In Fig. 12, we show the densities of scaled pressure, energy, entropy, and trace anomaly as functions of temperature at $\omega = 0.2$ GeV for different chemical potentials. A notable feature is that, in the low temperature region, the chemical potential can make a nontrivial contribution. It is shown that the pressure, energy density, and entropy density increase with temperature for different chemical potentials, and these quantities are also enhanced by the chemical potential. This enhancement can be readily understood, as a higher chemical potential activates more degrees of freedom. In the rotating system, the trace anomaly is enhanced by the chemical potential below the critical transition region, while across the transition region, it is suppressed. Additionally, with increasing chemical potential, the crossover shifts to lower transition temperatures. All the quantities in this figure exhibit a strong dependence on chemical potential below the crossover temperature. In Fig. 13, we show scaled specific heat and speed of sound squared as functions of temperature at $\omega = 0.2$ GeV for different chemical potentials. As shown in Fig. 13(a), scaled specific heat increases with temperature and reaches a peak at the chiral transition region. It then decreases rapidly around the critical chiral transition and eventually shows little variation with temperature. The figure shows that the peak shifts to lower temperatures as

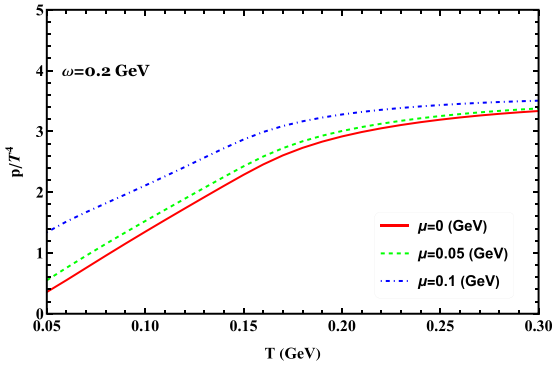

(a)

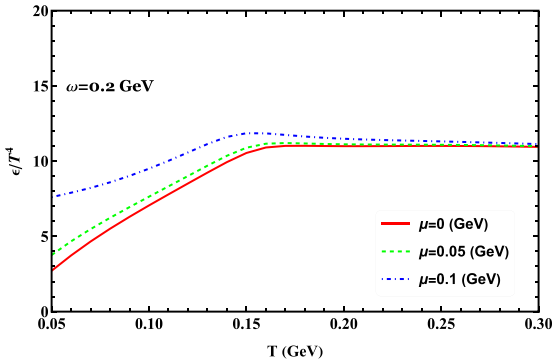

(b)

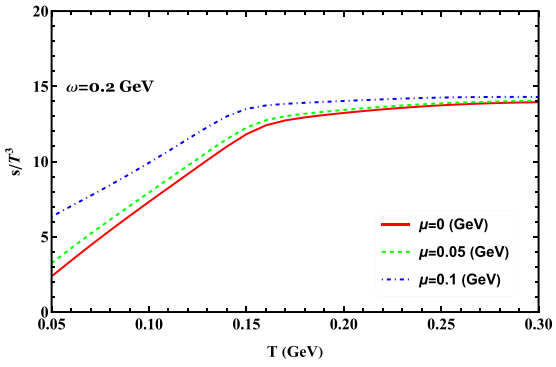

(c)

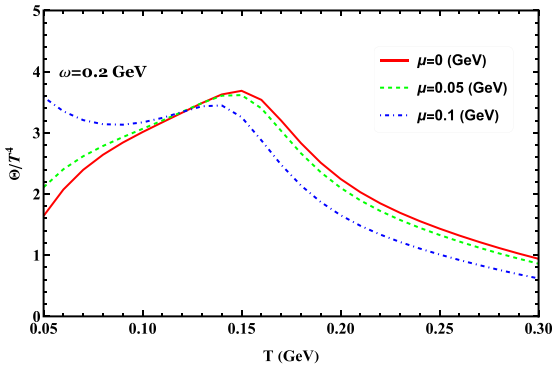

(d)

Fig. 12. (color online) Scaled pressure, energy density, entropy density, and trace anomaly as functions of temperature at $\omega = 0.2$ GeV for different chemical potentials.

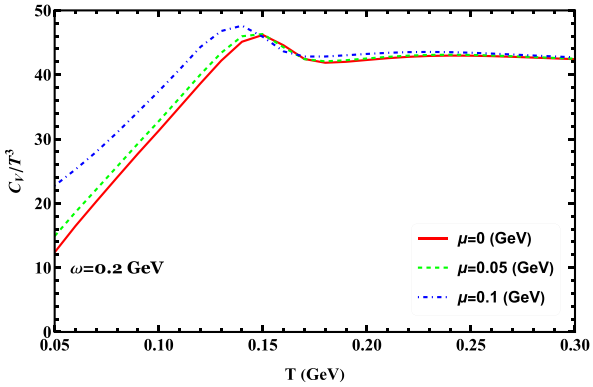

(a)

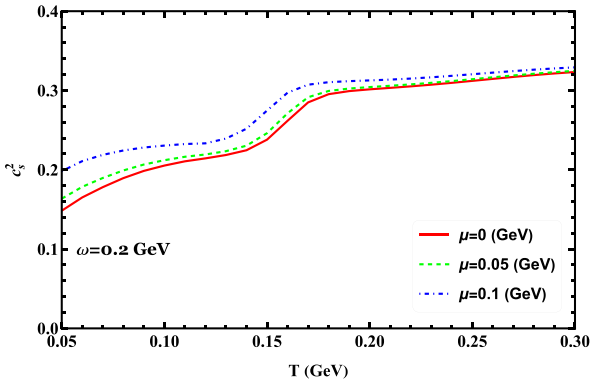

(b)

Fig. 13. (color online) Scaled specific heat and speed of sound squared as functions of temperature at $\omega = 0.2$ GeV for different chemical potentials.

the quark chemical potential increases. Fig. 13(b) shows a significant increase in the speed of sound squared with the quark chemical potential, even near the transition region. This suggests that finite chemical potential may have an important effect on the thermalization of QCD matter in a rotating system. Here, the speed of sound squared also conveys relevant information: it does not exhibit a local minimum at the crossover transition for the quark chemical potentials considered. This is owing to two facts: first, the system does not have an infinite volume as in the standard NJL model; second, the energy density is modified, *i.e.*, the addition of contributions from $J\omega$. It is clear that, as the chemical potential increases in the rotating system, a local minimum begins to emerge around the phase transition. The figure also shows that, in the high temperature limit, the speed of sound squared approaches the conformal limit of 1/3 for different angular velocities.

Another basic thermodynamic quantity is the angular momentum and moment of inertia. These quantities measure the breaking of conformal symmetry in the interaction theory. In Fig. 14, we show the scaled angular momentum and moment of inertia as functions of the temperature for different chemical potential at finite angular

velocities. They have similar characteristics as scaled quantities in Fig. 12 below the critical transition. As the temperature increases continuously, the scaled angular momentum gradually decreases, while the scaled moment of inertia consistently increases with temperature.

Another potential signature of the chiral transition is reflected in the behavior of the quark number densities. In Fig. 15, we show the scaled quark number density as a function of temperature at $\omega = 0.2$ GeV for different values of chemical potential. It can be concluded that, when the quark chemical potential equals zero, the corresponding quark number density is always zero. In the presence of finite quark chemical potential, the scaled quark number densities increase slightly until $T = 150$ MeV and decrease again with growing temperature. It is evident that the chemical potential enhances the quark number density in the rotating system.

E. Thermodynamics in rotating system at large angular velocity

In the following, we present a systematic analysis of the thermodynamic quantities of QCD matter under high angular velocity. The total pressure and energy density of the system during rotation are given by the sums of the contributions from each quark flavor. To provide a clearer picture of the effects of rotation on different quark flavors, we examine both the individual and total contributions.

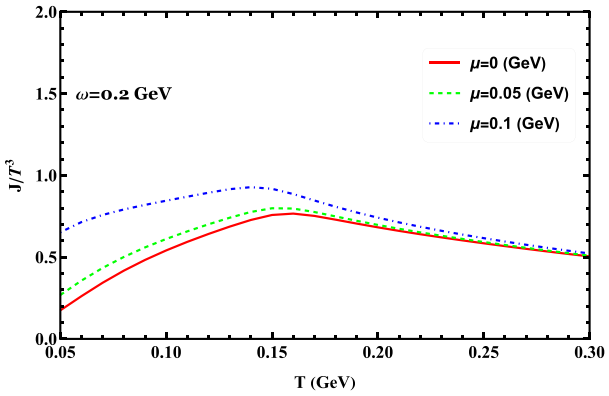

Fig. 14. (color online) Scaled angular momentum and moment of inertia as functions of temperature at $\omega = 0.2$ GeV for different chemical potentials.

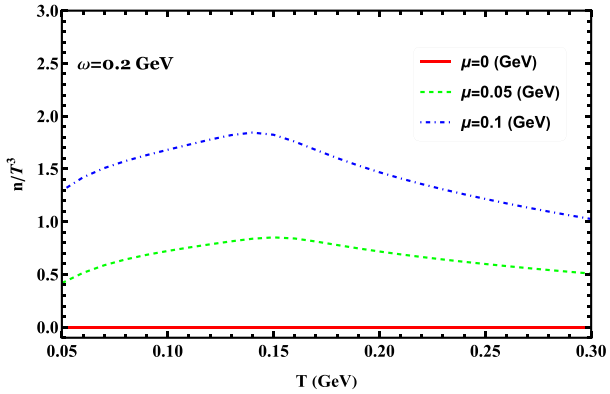

Fig. 15. (color online) Scaled quark number density as a function of temperature at $\omega = 0.2$ GeV for different values of chemical potential.

From the strong rotational behavior depicted in Fig. 16, it is evident that the bulk thermodynamic properties, such as scaled pressure, energy density, and trace anomaly, increase with angular velocity at a temperature of T=0.01 GeV and quark chemical potential $\mu = 0$GeV. Notably, the scaled pressure, energy density, and trace anomaly for both the light and strange quarks increase as the angular velocity rises. At mid-range angular velocities, below approximately 0.8 GeV, the light quark predominantly contributes to these thermodynamic quantities. However, at sufficiently high angular velocities, the contributions from different flavors become nearly equal. Note also that the angular momentum of the system exhibits a similar behavior in Fig. 17. It is evident that the angular momentum in the chiral broken phase is lower than in the chiral restored phase. Furthermore, the contribution of the light quark to the angular momentum is significant at mid-range angular velocities, while that of the strange quark is moderate.

There is a decline in the scaled entropy density after surpassing the critical point around $\omega = 0.6$ GeV because, in this region, the rate of increase in the quantity pressure slows down. Note also that there is a slight increase (not clearly visible in the figure) followed by a decrease in the entropy density around $\omega = 1.0$ GeV. The trace anomaly increases with angular velocity. This results from setting T=0.01 GeV; at such a low temperature, the strange quark remains in a phase with partially broken chiral symmetry. At higher temperatures, the trace anomaly becomes small.

We show the behavior of the scaled specific heat as a function of ω in T=0.01 GeV for vanishing chemical potential. The evolution of the scaled specific heat in-

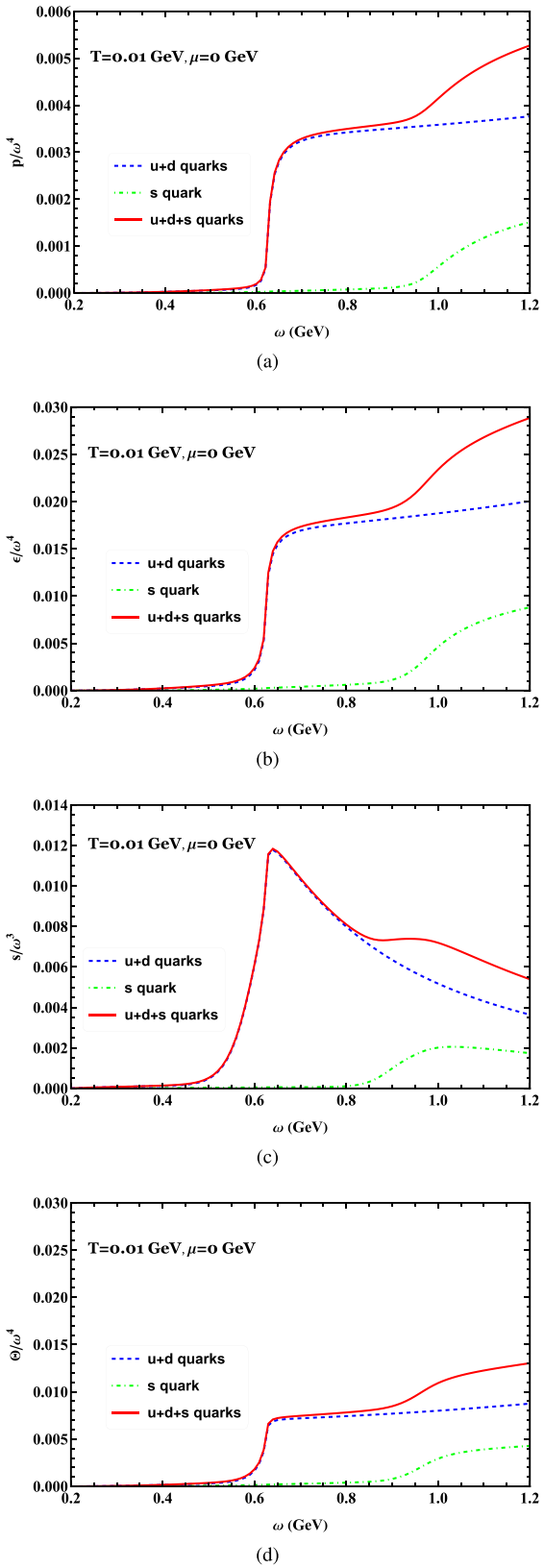

Fig. 16. (color online) Scaled pressure, energy density, entropy density, and trace anomaly as functions of angular velocity at T=0.01 GeV and $\mu = 0$ GeV for the light, strange, and total quarks, respectively.

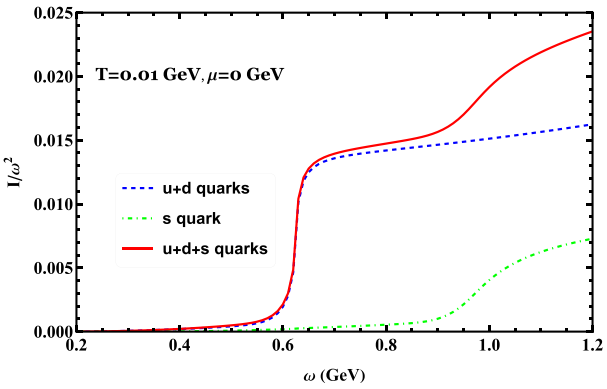

Fig. 17. (color online) Scaled moment of inertia as functions of angular velocity at T=0.01 GeV and $\mu = 0$ GeV for the light, strange, and total quarks, respectively.

creases from zero to a maximum value around $\omega = 0.6$ GeV. Then, it decreases to a minimum value and gradually increases to another sub-maximum value around $\omega = 1.0$ GeV. Finally, it gradually decreases at large angular velocity. From the figure, it can be concluded that the light quark density rises steeply across the chiral transition, while the strange quark exhibits a flatter peak over a relatively broad region. It is known that a sharp crossover, characterized by rapid changes in thermodynamic quantities over a small interval, increases the likelihood of measurable effects in experiments. Therefore, the specific heat may provide relevant signatures of phase transitions in the rotating system.

Figure 18(b) shows how the speed of sound squared varies with angular velocity for both light and strange quarks. It is known that, in the transition region of QCD matter, the speed of sound squared undergoes significant changes, showing a pronounced dip near the chiral transition. Its two local minima become deeper near the critical angular velocity, corresponding to the light and strange quarks, respectively. At low angular velocities, the speed of sound squared increases as the angular velocity rises. However, at high angular velocities, it subtly decreases with increasing angular velocity. Our numerical results suggest that the dependence of the speed of sound squared on the angular velocity can serve as an indicator of the QCD chiral transition. To probe this dependence further, we show the results of calculations for different temperatures in Fig. 19. This figure clearly illustrates the behavior of quark matter under rotation. It shows that the maximum value of the speed of sound is largely influenced by features associated with the chiral transitions. Additionally, the speed of sound squared increases with angular velocity in the low angular velocity region but decreases as the angular velocity increases in the high angular velocity region. At low angular velocities, there is a significant variation in the speed of sound across different temperatures. However, at high angular velocities, this variation diminishes, and the speed of sound con-

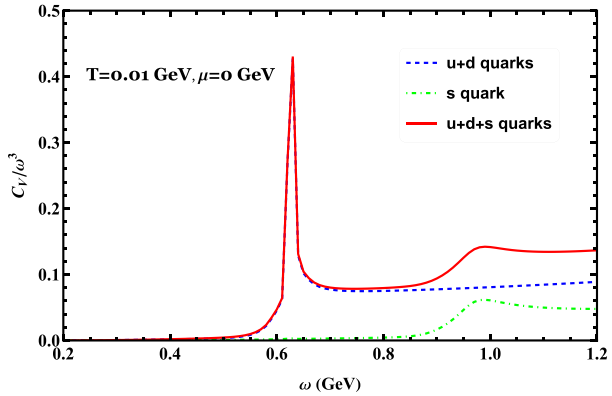

(a)

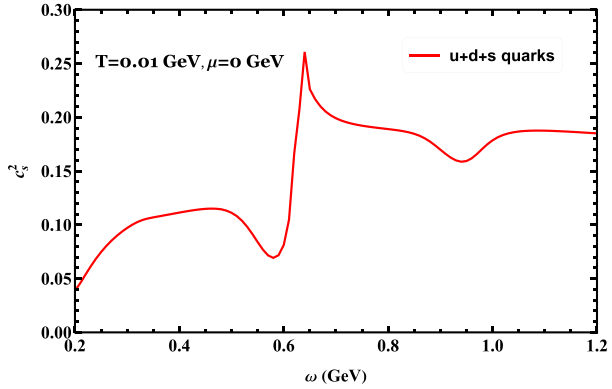

(b)

Fig. 18. (color online) (a) Scaled specific heat as a function of angular velocity at T=0.01 GeV and $\mu = 0$ GeV for the light, strange, and total quarks, respectively. (b) Corresponding results of speed of sound squared for the total quarks.

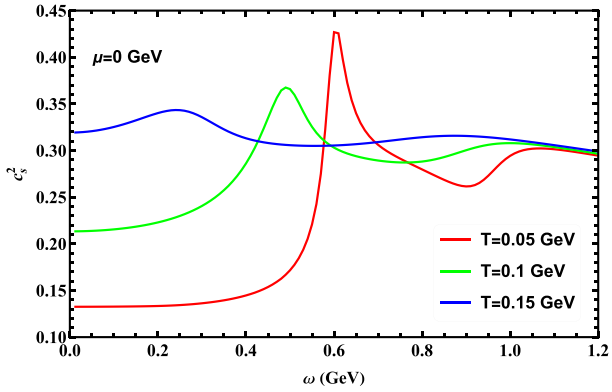

Fig. 19. (color online) Speed of sound squared as a function of angular velocity at $\mu = 0$ GeV for different temperatures.

verges to the same value. Thus, a key conclusion is that the speed of sound exhibits a nonmonotonic behavior as the angular velocity changes.

IV. CONCLUSIONS

To investigate the expansion of the plasma formed in ultra-relativistic heavy-ion collisions with noncentral impact, it is crucial to compute the thermodynamic properties within a rotating system. In this study, we focused on formulating and exploring the thermodynamics of the three-flavor NJL model under rotation. We present results for various thermodynamic observables as functions of temperature, considering different angular velocities, system radii, and finite quark chemical potentials. Additionally, we examined the thermodynamic behavior of light and strange quarks separately in relation to the angular velocity.

To summarize, we present an analytical approach for the thermodynamics in the three-flavor NJL model incorporating the effects of rotation. We systematically analyzed the equation of state in the parameter space of temperature T, chemical potential μ, and angular velocity ωin the rotational system. The calculations provide a clear picture of the chiral transition under rotation, indicating that rotation plays a significant role in the thermodynamics of QCD matter. By examining changes in thermodynamic quantities within a rotating system, we gained valuable insights into the properties and behavior of QCD matter. In such a system, scaled thermodynamic quantities are noticeably affected by rotation, with the moment of inertia showing a strong dependence on angular velocity even at high temperatures. The thermodynamic properties of light and heavy quarks differ across angular velocities, and this distinction significantly impacts the thermodynamic quantities. However, at sufficiently strong rotation, these flavor differences diminish. The speed of sound is a crucial quantity for studying thermodynamic properties and phase transitions in QGP. A key finding of our analysis is that the speed of sound squared exhibits a nonmonotonic behavior as a function of angular velocity.

It should be mentioned that, in the study of the properties of QCD matter, the effective volume effect and boundary conditions are crucial. They not only influence the phase structure and thermodynamic properties of QCD matter but also are closely related to experimental observations [90−103]. As demonstrated in Ref. [100], chiral condensation can exhibit either catalysis or inverse catalysis depending on the boundary conditions, with a quantized first-order phase transition appearing specifically under periodic boundary conditions. In Ref. [102], the finite size effect was taken into account under periodic, quasi-periodic, and anti-periodic boundary conditions. The results indicated that the phase structure of the system exhibited significant differences under different boundary conditions. For rotating QCD matter, the rotational system must satisfy the causality condition $\omega r < 1$. Thus, in principle, boundary conditions should be taken into account. In Ref. , it was found that, in the rotating system, the boundary effects can cause the quark chiral condensation to exhibit oscillatory behavior near the boundaries. In Ref. [104], lattice results on QCD matter

under rotation were investigated; three types of boundary conditions, namely open, periodic, and Dirichlet boundary conditions, were considered. In the holographic QCD model under rotation [103], the finite size effects and boundary conditions were discussed. Under Neumann or Dirichlet boundary conditions, different (inverse) catalysis effects on the chiral condensation occur. The finite volume effect, along with different boundary conditions, also influences the momentum distribution of particles in the system, thereby affecting its thermodynamic properties.

More importantly, finite volume effects and boundary conditions are closely related to experimental observations. In experiments such as heavy-ion collisions, the QCD matter produced exists under extreme conditions, with both its volume and boundary conditions being unique. Various phenomena observed in these experiments, such as particle production, distribution, and collective flow, are strongly influenced by finite volume effects and boundary conditions. Therefore, understanding the impact of these effects and conditions is crucial for connecting experimental results to the QCD phase diagram and thermodynamics. For simplicity, we did not consider boundary effects in this study, but we plan to carry out comprehensive and in-depth investigations in this area in the near future. Such research will not only deepen our theoretical understanding of strong interaction dynamics in rotating QCD systems but also provide a solid theoretical framework for interpreting and predicting phenomena observed in non-central heavy-ion collision experiments.

To date, we have developed the NJL model considering only fermion-antifermion scalar interactions for the chiral transition. It is important to note that vector interactions [105−107] may play a significant role in the chiral transition of the three-flavor NJL model in the presence of rotation. We leave this for further study. In addition, the Polyakov-Nambu-Jona-Lasinio (PNJL) model [108−114] incorporates the Polyakov loop integral based on the NJL model, considering the coupling between quark and gluon degrees of freedom. The PNJL model exhibits features of both chiral symmetry restoration and the deconfinement phase transition, which may enable it to better describe the properties of QCD matter under rotation at high temperatures and finite chemical potentials. The PNJL model under rotation was proposed in Refs. [21, 115]. Therefore, calculating the thermodynamic quantities within this model is meaningful. Although there remains some controversy regarding how rotation affects the deconfinement transition, we hope lattice QCD will provide further insights into the Polyakov loop. Finally, extending this research to the PNJL model will be an important future step.

ACKNOWLEDGEMENTS

We greatly thank Mei Huang, Jingfeng Liao, Yin Jiang, Kun Xu, and Jie Mei for useful discussions.

APPENDIX A: THERMODYNAMIC QUANTITIES

Next, we list detailed expressions for the entropy density, quark number density, and angular momentum along the z-axis:

$$s=\frac{3}{4\pi^2}\sum_f\sum_{n=-\infty}^{\infty}\int_0^{\infty}p_t\mathrm{d}p_t\int_{-\infty}^{\infty}\mathrm{d}p_z\left(\left(J_{n+1}(p_tr)^2+J_n(p_tr)^2\right)\times T\left\{\frac{\mathrm{e}^{-\frac{E_{f,n}-\mu_f}{T}}\left(E_{f,n}-\mu_f\right)}{\left(1+\mathrm{e}^{-\frac{E_{f,n}-\mu_f}{T}}\right)T^2}+\frac{\mathrm{e}^{-\frac{E_{f,n}+\mu_f}{T}}\left(E_{f,n}+\mu_f\right)}{\left(1+\mathrm{e}^{-\frac{E_{f,n}+\mu_f}{T}}\right)T^2}\right.\right.$$
$$\left.\left.+\log\left[1+\mathrm{e}^{-\frac{E_{f,n}-\mu_f}{T}}\right]+\log\left[1+\mathrm{e}^{-\frac{E_{f,n}+\mu_f}{T}}\right]\right\},\tag{A1}$$

$$n=\frac{3}{4\pi^2}\sum_f\sum_{n=-\infty}^{\infty}\int_0^{\infty}p_t\mathrm{d}p_t\int_{-\infty}^{\infty}\mathrm{d}p_z\left(\left(J_{n+1}(p_tr)^2+J_n(p_tr)^2\right)\times\frac{\mathrm{e}^{\frac{2M_f+\omega+2n\omega}{2T}}\left(-1+\mathrm{e}^{\frac{2\mu_f}{T}}\right)}{\left(\mathrm{e}^{\frac{M_f+\mu_f}{T}}+\mathrm{e}^{\frac{\left(\frac{1}{2}+n\right)\omega}{T}}\right)\left(\mathrm{e}^{\frac{M_f}{T}}+\mathrm{e}^{\frac{2\mu_f+\omega+2n\omega}{2T}}\right)}\right),\tag{A2}$$

$$J=\frac{3}{4\pi^2}\sum_{n=-\infty}^{\infty}\int_0^{\Lambda}p_t\mathrm{d}p_t\int_{-\sqrt{\Lambda^2-p_t^2}}^{\sqrt{\Lambda^2-p_t^2}}\mathrm{d}p_z\left(\left(J_{n+1}(p_tr)^2+J_n(p_tr)^2\right)(-1-2n)\right.$$
$$\left.+\frac{3}{4\pi^2}\sum_f\sum_{n=-\infty}^{\infty}\int_0^{\infty}p_t\mathrm{d}p_t\int_{-\infty}^{\infty}\mathrm{d}p_z\left(\left(J_{n+1}(p_tr)^2+J_n(p_tr)^2\right)\times\frac{\left(\mathrm{e}^{E_{f,n}/T}+2\mathrm{e}^{\frac{\mu_f}{T}}+\mathrm{e}^{\frac{E_{f,n}+2\mu_f}{T}}\right)(1+2n)}{2\left(\mathrm{e}^{E_{f,n}/T}+\mathrm{e}^{\frac{\mu_f}{T}}\right)\left(1+\mathrm{e}^{\frac{E_{f,n}+\mu_f}{T}}\right)}\right).\tag{A3}$$

References

[1] Z. T. Liang and X. N. Wang, Phys. Rev. Lett. **94**, 102301 (2005) [Erratum: Phys. Rev. Lett. **96**, 039901 (2006)], arXiv: nucl-th/0410079

[2] X. G. Huang, P. Huovinen, and X. N. Wang, Phys. Rev. C **84**, 054910 (2011), arXiv: 10.1108.5649[nucl-th]

[3] F. Becattini, F. Piccinini, and J. Rizzo, Phys. Rev. C **77**, 024906 (2008), arXiv: 10.0711.1253[nucl-th]

[4] W. T. Deng and X. G. Huang, Phys. Rev. C **93**, 064907 (2016), arXiv: 10.1603.06117[nucl-th]

[5] Y. Jiang, X. G. Huang, and J. Liao, Phys. Rev. D **92**, 071501 (2015), arXiv: 10.1504.03201[hep-ph]

[6] S. J. Barnett, Phys. Rev. **6**, 239 (1915)

[7] S. J. Barnett, Rev. Mod. Phys. **7**, 129 (1935)

[8] Y. Liu and I. Zahed, Phys. Rev. Lett. **120**, 032001 (2018), arXiv: 10.1711.08354[hep-ph]

[9] G. Cao and L. He, Phys. Rev. D **100**, 094015 (2019), arXiv: 10.1910.02728[nucl-th]

[10] H. L. Chen, X. G. Huang, and K. Mameda, JHEP **02**, 216 (2024), arXiv: 10.1910.02700[nucl-th]

[11] H. Zhang, D. Hou, and J. Liao, Chin. Phys. C **44**, 111001 (2020), arXiv: 10.1812.11787[hep-ph]

[12] G. Cao, Eur. Phys. J. C **81**, 148 (2021), arXiv: 10.2008.08321[nucl-th]

[13] H. L. Chen, K. Fukushima, X. G. Huang *et al.*, Phys. Rev. D **93**, 104052 (2016), arXiv: 10.1512.08974[hep-ph]

[14] Y. Jiang and J. Liao, Phys. Rev. Lett. **117**, 192302 (2016), arXiv: 10.1606.03808[hep-ph]

[15] S. Ebihara, K. Fukushima, and K. Mameda, Phys. Lett. B **764**, 94 (2017), arXiv: 10.1608.00336[hep-ph]

[16] M. N. Chernodub and S. Gongyo, JHEP **01**, 136 (2017), arXiv: 10.1611.02598[hep-th]

[17] M. N. Chernodub and S. Gongyo, Phys. Rev. D **95**, 096006 (2017), arXiv: 10.1702.08266[hep-th]

[18] X. Wang, M. Wei, Z. Li, and M. Huang*et al.*, Phys. Rev. D **99**, 016018 (2019), arXiv: 10.1808.01931[hep-ph]

[19] F. Sun and A. Huang, Phys. Rev. D **106**, 076007 (2022), arXiv: 10.2104.14382[hep-ph]

[20] K. Xu, F. Lin, A. Huang *et al.*, Phys. Rev. D **106**, L071502 (2022), arXiv: 10.2205.02420[hep-ph]

[21] F. Sun, K. Xu, and M. Huang, Phys. Rev. D **108**, 096007 (2023), arXiv: 10.2307.14402[hep-ph]

[22] X. Chen, L. Zhang, D. Li *et al.*, JHEP **07**, 132 (2021), arXiv: 10.2010.14478[hep-ph]

[23] Y. Fujimoto, K. Fukushima, and Y. Hidaka, Phys. Lett. B **816**, 136184 (2021), arXiv: 10.2101.09173[hep-ph]

[24] Y. Chen, X. Chen, D. Li *et al.*, (2024), arXiv: 2405.06386[hep-ph]

[25] L. Adamczyk *et al.* (STAR), Nature **548**, 62 (2017), arXiv: 1701.06657[nucl-ex]

[26] S. Acharya *et al.* (ALICE), Phys. Rev. Lett. **125**, 012301 (2020), arXiv: 1910.14408[nucl-ex]

[27] M. S. Abdallah *et al.* (STAR), Nature **614**, 244 (2023), arXiv: 2204.02302[hep-ph]

[28] V. V. Braguta, A. Kotov, A. Roenko *et al.*, PoS **LATTICE2022**, 190 (2023), arXiv: 2212.03224[hep-lat]

[29] M. N. Chernodub, V. A. Goy, and A. V. Molochkov, Phys. Rev. D **107**, 114502 (2023), arXiv: 10.2209.15534[hep-lat]

[30] V. V. Braguta, M. N. Chernodub, A. A. Roenko *et al.*, (2023), arXiv: 2303.03147[hep-lat]

[31] V. V. Braguta, I. E. Kudrov, A. A. Roenko *et al.*, JETP Lett. **117**, 639 (2023)

[32] J. C. Yang and X. G. Huang, (2023), arXiv: 2307.05755 [heplat]

[33] L. P. Csernai, V. K. Magas, and D. J. Wang, Phys. Rev. C **87**, 034906 (2013), arXiv: 10.1302.5310[nucl-th]

[34] F. Becattini, L. Csernai, and D. J. Wang, Phys. Rev. C **88**, 034905 (2013) [Erratum: Phys. Rev. C **93**, 069901 (2016)], arXiv: 1304.4427[nucl-th]

[35] L. P. Csernai, S. Velle, and D. J. Wang, Phys. Rev. C **89**, 034916 (2014), arXiv: 10.1305.0396[nucl-th]

[36] L. P. Csernai, D. J. Wang, M. Bleicher *et al.*, Phys. Rev. C **90**, 021904 (2014)

[37] L. P. Csernai, D. J. Wang, and T. Csorgo, Phys. Rev. C **90**, 024901 (2014), arXiv: 10.1406.1017[hep-ph]

[38] F. Becattini, G. Inghirami, V. Rolando *et al.*, Eur. Phys. J. C **75**, 406 (2015) [Erratum: Eur. Phys. J. C **78**, 354 (2018)], arXiv: 1501.04468[nucl-th]

[39] Y. Xie, R. C. Glastad, and L. P. Csernai, Phys. Rev. C **92**, 064901 (2015), arXiv: 10.1505.07221[nucl-th]

[40] Y. L. Xie, M. Bleicher, H. Stöcker *et al.*, Phys. Rev. C **94**, 054907 (2016), arXiv: 10.1610.08678[nucl-th]

[41] I. Karpenko and F. Becattini, Eur. Phys. J. C **77**, 213 (2017), arXiv: 10.1610.04717[nucl-th]

[42] Y. Xie, D. Wang, and L. P. Csernai, Phys. Rev. C **95**, 031901 (2017), arXiv: 10.1703.03770[nucl-th]

[43] Y. Xie, G. Chen, and L. P. Csernai, Eur. Phys. J. C **81**, 12 (2021), arXiv: 10.1912.00209[hep-ph]

[44] Y. B. Ivanov, V. D. Toneev, and A. A. Soldatov, Phys. Rev. C **100**, 014908 (2019), arXiv: 10.1903.05455[nucl-th]

[45] Y. B. Ivanov and A. A. Soldatov, Phys. Rev. C **102**, 024916 (2020), arXiv: 10.2004.05166[nucl-th]

[46] F. Becattini, M. Buzzegoli, G. Inghirami *et al.*, Phys. Rev. Lett. **127**, 272302 (2021), arXiv: 10.2103.14621[nucl-th]

[47] S. Wu and Y. Xie, Eur. Phys. J. A **59**, 108 (2023), arXiv: 10.2303.07680[nucl-th]

[48] Y. Jiang, Z. W. Lin, and J. Liao, Phys. Rev. C **94**, 044910 (2016) [Erratum: Phys. Rev. C **95**, 049904 (2017)], arXiv: 1602.06580[hep-ph]

[49] L. G. Pang, H. Petersen, Q. Wang *et al.*, Phys. Rev. Lett. **117**, 192301 (2016), arXiv: 10.1605.04024[hep-ph]

[50] H. Li, L. G. Pang, Q. Wang *et al.*, Phys. Rev. C **96**, 054908 (2017), arXiv: 10.1704.01507[nucl-th]

[51] S. Shi, K. Li, and J. Liao, Phys. Lett. B **788**, 409 (2019), arXiv: 10.1712.00878[nucl-th]

[52] I. Karpenko and F. Becattini, Nucl. Phys. A **967**, 764 (2017), arXiv: 10.1704.02142[nucl-th]

[53] X. L. Xia, H. Li, Z. B. Tang *et al.*, Phys. Rev. C **98**, 024905 (2018), arXiv: 10.1803.00867[nucl-th]

[54] D. X. Wei, W. T. Deng, and X. G. Huang, Phys. Rev. C **99**, 014905 (2019), arXiv: 10.1810.00151[nucl-th]

[55] O. Vitiuk, L. V. Bravina, and E. E. Zabrodin, Phys. Lett. B **803**, 135298 (2020), arXiv: 10.1910.06292[hep-ph]

[56] Y. Guo, S. Shi, S. Feng *et al.*, Phys. Lett. B **798**, 134929 (2019), arXiv: 10.1905.12613[nucl-th]

[57] R. Campanini and G. Ferri, Phys. Lett. B **703**, 237 (2011), arXiv: 10.1106.2008[hep-ph]

[58] F. G. Gardim, G. Giacalone, M. Luzum *et al.*, Nature Phys. **16**, (2020), arXiv: 10.1908.09728[nucl-th]
[59] F. G. Gardim, G. Giacalone, and J. Y. Ollitrault, Phys. Lett. B **809**, 135749 (2020), arXiv: 10.1909.11609[nucl-th]
[60] A. Sorensen, D. Oliinychenko, V. Koch *et al.*, Phys. Rev. Lett. **127**, 042303 (2021), arXiv: 10.2103.07365[nuclth]
[61] A. Hayrapetyan *et al.* (CMS), (2024), arXiv: 2401.06896[nucl-ex]
[62] P. Parotto, M. Bluhm, D. Mroczek *et al.*, Phys. Rev. C **101**, 034901 (2020), arXiv: 10.1805.05249[hep-ph]
[63] A. Monnai, B. Schenke, and C. Shen, Int. J. Mod. Phys. A **36**, 2130007 (2021), arXiv: 10.2101.11591[nucl-th]
[64] Q. Chen, R. Wen, S. Yin *et al.*, (2024), arXiv: 2402.12823 [nucl-th]
[65] Y. f. Shen, W. Chen, X. y. Wu *et al.*, (2024), arXiv: 2404.02397 [hep-ph]
[66] P. O. Bowman, U. M. Heller, D. B. Leinweber *et al.*, Phys. Rev. D **70**, 034509 (2004), arXiv: 10. hep-lat/0402032
[67] A. Sternbeck, E. M. Ilgenfritz, M. Muller-Preussker *et al.*, PoS **LAT2006**, 076 (2006), arXiv: hep-lat/0610053
[68] W. j. Fu, J. M. Pawlowski, and F. Rennecke, Phys. Rev. D **101**, 054032 (2020), arXiv: 10.1909.02991[hep-ph]
[69] J. Braun, L. Fister, J. M. Pawlowski *et al.*, Phys. Rev. D **94**, 034016 (2016), arXiv: 10.1412.1045[hep-ph]
[70] M. Mitter, J. M. Pawlowski, and N. Strodthoff, Phys. Rev. D **91**, 054035 (2015), arXiv: 10.1411.7978[hep-ph]
[71] A. K. Cyrol, M. Mitter, J. M. Pawlowski *et al.*, Phys. Rev. D **97**, 054006 (2018), arXiv: 10.1706.06326[hep-ph]
[72] Y. Nambu and G. Jona-Lasinio, Phys. Rev. **122**, 345 (1961)
[73] Y. Nambu and G. Jona-Lasinio, Phys. Rev. **124**, 246 (1961)
[74] S. P. Klevansky, Rev. Mod. Phys. **64**, 649 (1992)
[75] T. Hatsuda and T. Kunihiro, Phys. Rept. **247**, 221 (1994), arXiv: 10. hep-ph/9401310
[76] M. Buballa, Phys. Rept. **407**, 205 (2005), arXiv: hepph/0402234
[77] B.-J. Schaefer and J. Wambach, Nucl. Phys. A **757**, 479 (2005), arXiv: 10. nucl-th/0403039
[78] B. J. Schaefer, J. M. Pawlowski, and J. Wambach, Phys. Rev. D **76**, 074023 (2007), arXiv: 10.0704.3234[hep-ph]
[79] R. Wen, C. Huang, and W. J. Fu, Phys. Rev. D **99**, 094019 (2019), arXiv: 10.1809.04233[hep-ph]
[80] A. Yamamoto and Y. Hirono, Phys. Rev. Lett. **111**, 081601 (2013), arXiv: 10.1303.6292[hep-lat]
[81] H. L. Chen, Z. B. Zhu, and X. G. Huang, Phys. Rev. D **108**, 054006 (2023), arXiv: 10.2306.08362[hep-ph]
[82] A. L. Fetter, Rev. Mod. Phys. **81**, 647 (2009)
[83] J. I. Kapusta and C. Gale, *Finite-Temperature Field Theory: Principles and Applications*, 2nd ed., Cambridge Monographs on Mathematical Physics (Cambridge University Press, 2006)
[84] L. Landau and E. Lifshitz, *Course of Theoretical Physics. Vol. 5: Statistical Physics*, Part 1 (Butterworth-Heinemann, Oxword U.K., 1980)
[85] Y. Q. Zhao, S. He, D. Hou *et al.*, JHEP **04**, 115 (2023), arXiv: 10.2212.14662[hep-ph]
[86] H. Kohyama, D. Kimura, and T. Inagaki, Nucl. Phys. B **906**, 524 (2016), arXiv: 10.1601.02411[hep-ph]
[87] A. Bhattacharyya, P. Deb, S. K. Ghosh *et al.*, Phys. Rev. D **87**, 054009 (2013), arXiv: 10.1212.5893[hep-ph]
[88] B. Klein, Physics Reports **707-708**, 1 (2017), modeling FiniteVolume Effects and Chiral Symmetry Breaking in Two-Flavor QCD Thermodynamics
[89] J. H. Wang and S. Q. Feng, Phys. Rev. D **109**, 066019 (2024), arXiv: 10.2403.01814[hep-ph]
[90] J. Braun, B. Klein, and H. J. Pirner, Phys. Rev. D **72**, 034017 (2005)
[91] J. Braun, B. Klein, H. J. Pirner *et al.*, Phys. Rev. D **73**, 074010 (2006)
[92] O. Kiriyama, T. Kodama, and T. Koide, (2006)
[93] G. y. Shao, L. Chang, Y. x. Liu *et al.*, Phys. Rev. D **73**, 076003 (2006)
[94] L. F. Palhares, E. S. Fraga, and T. Kodama, J. Phys. G **38**, 085101 (2011)
[95] J. Braun, B. Klein, and B. J. Schaefer, Phys. Lett. B **713**, 216 (2012)
[96] G. Almasi, R. Pisarski, and V. Skokov, Phys. Rev. D **95**, 056015 (2017)
[97] B. Klein, Phys. Rept. **707-708**, 1 (2017)
[98] Q. W. Wang, Y. Xia, C. Shi *et al.*, (2018)
[99] B. L. Li, Z. F. Cui, B. W. Zhou *et al.*, Nucl. Phys. B **938**, 298 (2019)
[100] K. Xu and M. Huang, Phys. Rev. D **101**, 074001 (2020)
[101] Y. P. Zhao, P. L. Yin, Z. H. Yu *et al.*, Nucl. Phys. B **952**, 114919 (2020)
[102] E. B. S. Corrêa and M. S. R. Sarges, Nucl. Phys. A **1040**, 122749 (2023)
[103] Y. Chen, D. Li, and M. Huang, Phys. Rev. D **106**, 106002 (2022), arXiv: 10.2208.05668[hep-ph]
[104] V. V. Braguta, A. Y. Kotov, D. D. Kuznedelev *et al.*, Phys. Rev. D **103**, 094515 (2021), arXiv: 10.2102.05084[hep-lat]
[105] M. Asakawa and K. Yazaki, Nucl. Phys. A **504**, 668 (1989)
[106] S. Klimt, M. F. M. Lutz, and W. Weise, Phys. Lett. B **249**, 386 (1990)
[107] M. Buballa, Nucl. Phys. A **611**, 393 (1996), arXiv: 10. nuclth/9609044
[108] P. N. Meisinger and M. C. Ogilvie, Phys. Lett. B **379**, 163 (1996), arXiv: 10. hep-lat/9512011
[109] P. N. Meisinger, T. R. Miller, and M. C. Ogilvie, Phys. Rev. D **65**, 034009 (2002), arXiv: 10. hep-ph/0108009
[110] K. Fukushima, Phys. Lett. B **591**, 277 (2004), arXiv: 10. hepph/0310121
[111] A. Mocsy, F. Sannino, and K. Tuominen, Phys. Rev. Lett. **92**, 182302 (2004), arXiv: 10. hep-ph/0308135
[112] E. Megias, E. Ruiz Arriola, and L. L. Salcedo, Phys. Rev. D **74**, 065005 (2006), arXiv: 10. hep-ph/0412308
[113] C. Ratti, M. A. Thaler, and W. Weise, Phys. Rev. D **73**, 014019 (2006), arXiv: 10. hep-ph/0506234
[114] K. Fukushima, Phys. Rev. D **77**, 114028 (2008) [Erratum: Phys. Rev. D **78**, 039902 (2008)], arXiv: 0803.3318[hep-ph]
[115] F. Sun, J. Shao, R. Wen *et al.*, Phys. Rev. D **109**, 116017 (2024), arXiv: 10.2402.16595[hep-ph]